JACS
JOURNAL OF THE AMERICAN CHEMICAL SOCIETY
Article
pubs.acs.org/JACS

The Formation of Highly Oxidized Multifunctional Products in the Ozonolysis of Cyclohexene

Matti P. Rissanen,*[,†] Theo Kurtén,[‡] Mikko Sipilä,[†] Joel A. Thornton,[§] Juha Kangasluoma,[†] Nina Sarnela,[†] Heikki Junninen,[†] Solvejg Jørgensen,[∥] Simon Schallhart,[†] Maija K. Kajos,[†] Risto Taipale,[†] Monika Springer,[⊥] Thomas F. Mentel,[⊥] Taina Ruuskanen,[†] Tuukka Petäjä,[†] Douglas R. Worsnop,[†,#] Henrik G. Kjaergaard,[∥] and Mikael Ehn[†]

[†]Department of Physics, University of Helsinki, P.O. Box 64, Helsinki, 00014, Finland
[‡]Department of Chemistry, University of Helsinki, P.O. Box 55, Helsinki, 00014, Finland
[§]Department of Atmospheric Sciences, University of Washington, Seattle, Washington 98195, United States
[∥]Department of Chemistry, University of Copenhagen, Universitetsparken 5, 2100 Copenhagen Ø, Denmark
[⊥]Institute for Energy and Climate Research (IEK-8), Forschungszentrum Jülich, 52425 Jülich, Germany
[#]Aerodyne Research Inc., 45 Manning Road, Billerica, Massachusetts 01821, United States

Supporting Information

ABSTRACT: The prompt formation of highly oxidized organic compounds in the ozonolysis of cyclohexene (C_6H_{10}) was investigated by means of laboratory experiments together with quantum chemical calculations. The experiments were performed in borosilicate glass flow tube reactors coupled to a chemical ionization atmospheric pressure interface time-of-flight mass spectrometer with a nitrate ion (NO_3^-)-based ionization scheme. Quantum chemical calculations were performed at the CCSD(T)-F12a/VDZ-F12//ωB97XD/aug-cc-pVTZ level, with kinetic modeling using multiconformer transition state theory, including Eckart tunneling corrections. The complementary investigation methods gave a consistent picture of a formation mechanism advancing by peroxy radical (RO_2) isomerization through intramolecular hydrogen shift reactions, followed by sequential O_2 addition steps, that is, RO_2 autoxidation, on a time scale of seconds. Dimerization of the peroxy radicals by recombination and cross-combination reactions is in competition with the formation of highly oxidized monomer species and is observed to lead to peroxides, potentially diacyl peroxides. The molar yield of these highly oxidized products (having O/C > 1 in monomers and O/C > 0.55 in dimers) from cyclohexene ozonolysis was determined as (4.5 ± 3.8)%. Fully deuterated cyclohexene and *cis*-6-nonenal ozonolysis, as well as the influence of water addition to the system (either H_2O or D_2O), were also investigated in order to strengthen the arguments on the proposed mechanism. Deuterated cyclohexene ozonolysis resulted in a less oxidized product distribution with a lower yield of highly oxygenated products and *cis*-6-nonenal ozonolysis generated the same monomer product distribution, consistent with the proposed mechanism and in agreement with quantum chemical modeling.

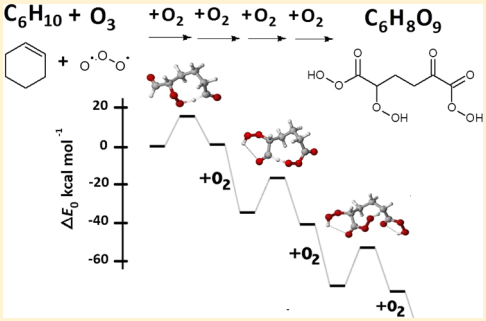

1. INTRODUCTION

Understanding the gas-phase oxidation of hydrocarbons is a fundamental prerequisite for controlling and optimizing many important physicochemical processes. For example, the amount of utilizable energy from combustion of a fossil fuel, or any other organic compound, is ultimately governed by the amount of energy released by breaking its carbon−carbon (C−C) and carbon−hydrogen (C−H) bonds while oxidizing the carbon to CO_2. In the atmosphere, the oxidation of biogenic and anthropogenic hydrocarbon emissions can lead to the formation and growth of aerosol particles by gas-to-particle conversion of the lower volatility products, and thus influence climate, ecosystem function, and human health.[1−13]

Autoxidation of organic compounds by peroxy radical isomerization through intramolecular hydrogen-shift reactions is a well-known reaction pathway in low-temperature combustion chemistry,[14−16] and is known to occur in various other environments too.[17−25] Recently, the autoxidation phenomenon was proposed to be a significant route for gas-phase oxidation of volatile organic compounds (VOCs) in the ambient atmosphere in low-NO_x conditions, especially for VOCs related to the formation of secondary organic aerosol.[19,20]

Ehn et al.[12] reported a large source of low-volatility secondary organic aerosol (SOA) generated from the ozonolysis of α-pinene and other endocyclic monoterpenes. The detection of highly oxygenated and high molecular weight

Received: July 15, 2014
Published: October 6, 2014

   dx.doi.org/10.1021/ja507146s | J. Am. Chem. Soc. 2014, 136, 15596−15606

Scheme 1[a]

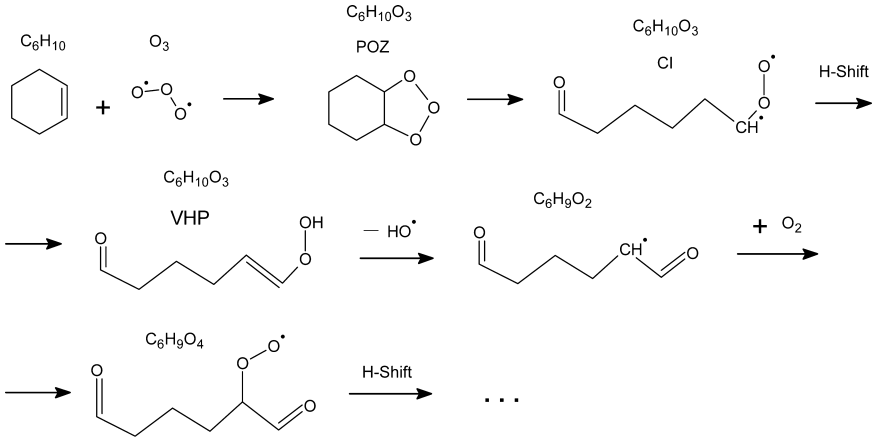

[a]Ozonolysis of cyclohexene produces a primary ozonide (POZ) that instantly decomposes to one of two identical Criegee intermediates (CI). The CI promptly isomerizes to a vinylhydroperoxide (VHP), which subsequently dissociates, losing an OH-radical. This creates a carbon-centered radical ($C_6H_9O_2$) which is able to add an O_2 molecule to form an oxygen-centered peroxy radical ($C_6H_9O_4$), which can isomerize yet further.

products in the gas-phase during ozonolysis under atmospheric conditions explained a significant fraction of the condensed-phase mass. Also Zhao et al.[26] reached similar conclusions in their chamber investigation of the α-pinene ozonolysis system. These extremely low volatility organic compounds (ELVOCs[9,12,27]) were previously detected as natural ions measured at a boreal forest measurement station (SMEAR II) in Hyytiälä, Finland,[28] but the formation mechanisms were unknown. Ehn et al.[12] proposed, on the basis of the behavior of several of the detected peroxy radical intermediates and products, that the mechanism of ELVOC formation was driven by RO_2 autoxidation.

Because of its structural similarity with abundant biogenic monoterpenes, cyclohexene (unsaturated, endocyclic C_6H_{10}) has been extensively studied as a monoterpene surrogate for inferring oxidation mechanisms and aerosol formation characteristics.[29−57] Ozonolysis is a common removal pathway for unsaturated compounds in the atmosphere, and because of the high reaction exothermicities, is known to lead to an ensemble of reactive intermediates.[17,39,58,59] From these the most attention has been centered on stabilized Criegee intermediates (sCI; a Criegee intermediate capable of reacting in a bimolecular reaction) owing to their potential important role as an oxidant and source of low volatility carboxylic acids and acid esters.[17,59−61] The cyclohexene ozonolysis reaction, however, is not expected to lead to a sCI,[35,36] but instead, is expected to isomerize promptly to another reactive intermediate: the vinylhydroperoxide (VHP).[30,36,39] The VHP formed is generally susceptible to dissociation to an OH and an organic oxygenated radical. This oxygenated radical is the potential precursor to a sequence of reactions leading to ELVOC species, and hence, is in the focus of this work.

In previous experiments the cyclohexene ozonolysis was shown to produce an ELVOC product distribution,[12] and in the present investigation we aimed to explore more completely how these highly oxidized ELVOCs are formed—in a step-by-step manner. We show by detailed experimental investigation, together with high-level quantum chemical calculations, how the oxygen is infused to the organic carbon structures by sequential O_2 addition + peroxy radical isomerization steps. The radical chain process is eventually terminated by ejection of an OH or HO_2 radical, or by bimolecular reactions with other peroxy radicals, forming the ELVOC product. In addition to the cyclohexene model system (unsubstituted, cyclic C_6H_{10}), we also studied the fully deuterated isotopologue (C_6D_{10}) as well as H/D-exchange reactions by adding D_2O to the gas flow, to further clarify the mechanism. As a final test on the general applicability of the proposed mechanism, we performed *cis*-6-nonenal (linear $CH_3CH_2CH{=}CH(CH_2)_4CHO$) ozonolysis experiments, which should produce the same VHP intermediate, and hence, the same ELVOC product distribution.

2. EXPERIMENTAL SECTION

2.1. Laboratory Investigations. ELVOC detection was performed with a chemical ionization atmospheric pressure interface time-of-flight (CI-APi-TOF) mass spectrometer using a nitrate ion (NO_3^-)-based chemical ionization scheme where ELVOCs form adducts with NO_3^-. The organic precursor concentrations were retrieved by a proton transfer reaction time-of-flight mass spectrometer (PTR-TOF-MS) or were calculated from the measured gas flow rates. Both of the mass spectrometers and their basic measurement routines have been described previously[62−66] and thus only a brief overview is given in the Supporting Information (SI).

The ozonolysis reactions of C_6H_{10}, C_6D_{10}, and $C_9H_{16}O$ (=*cis*-6-nonenal) were investigated in two different borosilicate glass flow tube reactors: a 205 cm long with a 4.7 cm i.d. and a 63 cm long with a 4.0 cm i.d., respectively. All experiments were performed under laminar flow conditions, at room temperature (T = 293 ± 3 K) and at ambient pressure using nitrogen (N_2) or synthetic air (N_2 and O_2) as the bath gas. Ozone and organic precursor concentrations, and their residence time in the reactor, were varied between different experiments. Measurements were also conducted with different amounts of water (H_2O) and deuterated water (D_2O) in the reaction mixture. The O_3 was produced from synthetic air by an ozone generator (Dasibi 1008-PC) and the concentration was quantified by an ozone analyzer (Thermo Scientific model 49). Water (H_2O or D_2O) was added to the gas stream by bubbling a variable part of the bath gas flow through a water reservoir. The amount of water in the gas flow was not quantified further. For more details about the setup and description of the different experiments performed see the Supporting Information (Figure S1 and Table S1).

2.2. Quantum Chemical Computations. Quantum chemical calculations were used to investigate the first three sequential hydrogen shifts for the peroxy radical formed after the VHP decomposition in the ozonolysis of cyclohexene ($C_6H_9O_4$, see Scheme 1). As discussed for example in Ehn et al.[12] and references therein, the first hydrogen shift very likely takes place at the carbonyl group

dx.doi.org/10.1021/ja507146s | J. Am. Chem. Soc. 2014, 136, 15596−15606

opposite the peroxy group. The second hydrogen shift can then occur either at the remaining carbonyl (a 1,8 H-shift) or at the COOH carbon (a 1,7 H-shift), the latter leading to a termination of the radical reaction chain through OH elimination.[19,20,67] If the second H-shift takes place at the carbonyl group, a third H-shift can then occur. For this third step we studied all four possible abstraction sites (though only the fastest two were selected for further analysis as the conformational sampling of the products was extremely time-consuming).

An initial set of conformers for each reactant, transition state and product structure were generated with the systematic conformer search algorithm of Spartan (versions 08, 12, and 14),[68] using the MMFF and Sybyl force-fields. The systematic algorithm explores all possible combinations of torsional angles, leading to over 100 000 trial structures for the larger systems in this study. Two different force-field methods were used as they predicted different hydrogen-bonding patterns, and we wanted to make sure all possible conformers are included in the sampling. For some structures (the carbon-centered radical products of the second and third peroxy radical H-shifts, as well as the second CO loss transition state, see Scheme 2 below) the Sybyl force field predicted chemically unreasonable structures, for example, with C−C·−H bond angles below 90 deg (C· is the radical center carbon atom). In these cases, additional conformers were generated either by reoptimizing the Sybyl-generated structures using the AM1 semiempirical method, or by generating a set of new conformers using the Monte Carlo sampling algorithm with the AM1 method if the previous approach failed.

The energies of the force-field optimized conformers (which numbered between 100 and 6000 per system; as many initial combinations of torsion angles did not lead to distinct minima) were subsequently evaluated at the B3LYP/6-31+G(d) level using the Spartan program. The conformers were then ordered by the B3LYP single-point energy, and those within either 3, 4, or 5 kcal/mol of the lowest-energy structure were chosen for B3LYP/6-31+G(d) optimizations, again using the Spartan program.[69] The cutoff was selected to keep the number of structure optimizations reasonable (i.e., less than 300). We emphasize that whenever a cutoff lower than 5 kcal/mol was used, several hundred different conformers were still optimized at the B3LYP/6-31+G(d) level, providing a quite extensive conformational sampling.

For sampling the transition state conformers, key parameters of the reacting groups (−C−H···O−O−) were constrained ("frozen") in the force field and B3LYP optimizations. These were the C−H and H···O and O−O distances for the hydrogen shifts, and the C−C═O distance for the CO loss reactions. The values for the parameters were determined on the basis of an initial B3LYP/6-31+G(d) transition-state optimization for a randomly chosen conformer for each transition state. Test calculations on the first H-shift transition state conformers indicate that the relevant distances and angles change very little from one conformer (of the same transition state type) to another, and the B3LYP relative energy changed by less than 0.25 kcal/mol (and typically less than 0.1 kcal/mol) upon relaxation of the constraints in a subsequent transition state optimization. Using constraints was necessary for the force-field conformational search to work, as these methods are unable to treat bond breaking and formation. Using them also in the B3LYP optimization stage allowed us to use minimization (rather than transition state search) algorithms in the conformational sampling. This significantly reduces the computational effort, and allowed us to sample a much larger number of transition state conformers.

Next, the B3LYP-optimized structures were again ordered by energy, and those within 2 kcal/mol of the lowest energy structure were chosen for subsequent optimization at the ωB97XD/aug-cc-pVTZ level[70] using the Gaussian 09 program suite,[71] tight optimization criteria and the ultrafine integration grid. The total number of structures optimized at this level in this study was over 500. For each system (reactant, transition state, or product), the conformer with the lowest zero-point corrected energy at the ωB97XD/aug-cc-pVTZ level, was then selected, and a final single-point energy calculation was carried out at the ROHF-RCCSD(T)-F12a/VDZ-F12 level,[72,73] using the Molpro 2012 program.[74] Intrinsic reaction coordinate (IRC) calculations on the lowest zero-point corrected energy transition state conformers were carried out at the ωB97XD/aug-cc-pVTZ level for at least 40 points in each direction to verify that the transition states connect the correct reactant and product systems. See section S2.1 in the Supporting Information for further validation of the conformational sampling algorithm.

The rate coefficients for the forward and reverse hydrogen shift as well as the forward rate coefficients for the CO loss reactions (assumed to be irreversible) were estimated using multiconformer transition state theory (MC-TST).[75] The MC-TST rate coefficient is given by

$$k_{\mathrm{MC-TST}} = \Gamma \frac{k_B T}{h} \frac{Q_{\mathrm{TS}}}{Q_{\mathrm{R}}} \exp\left(-\frac{E_{0,\mathrm{TS}} - E_{0,\mathrm{R}}}{RT}\right) \quad (1)$$

where Q_R and Q_{TS} are the partition functions for the reactant, R, and the transition state, TS, respectively, defined in eq 2. The energy $E_{0,TS}$ ($E_{0,R}$) corresponds to the zero-point corrected ROHF-RCCSD(T)-F12a/VDZ-F12//ωB97XD/aug-cc-pVTZ electronic energy for the lowest-energy conformer. The constants h, k_B, R, and T are the Planck constant, the Boltzmann constant, the gas constant, and the temperature, respectively. The temperature is set to 298.15 K.

We extracted the partition function, electronic energy, and zero point vibrational energy from all the conformers optimized at the ωB97XD/aug-cc-pVTZ level. The calculations of the partition functions are based on the standard rigid rotor and harmonic oscillation approximations. The partition function is given as

$$Q = \sum_{i=0}^{N-1} Q_{\mathrm{vib},i} Q_{\mathrm{rot},i} \exp\left(-\frac{E_i - E_0}{RT}\right) \quad (2)$$

where N is the number of conformers included, and E_i is the zero-point corrected energy of conformer i at the ωB97XD/aug-cc-pVTZ level. The energy of the lowest lying conformer is denoted by E_0.

The quantum tunneling correction, Γ, is computed with a one-dimensional Eckart correction model.[76] The tunneling corrections have only been computed for the conformers (reactant, transition state, and product) with the lowest zero-point corrected energy. We have used the ROHF-RCCSD(T)-F12a/VDZ-F12 energies to compute the barrier heights for the forward and reverse barriers, and the ωB97XD/aug-cc-pVTZ imaginary frequencies of the transition states. For a comparison of conventional transition state theory (TST) and MC-TST rate coefficients and partition functions, see section S2.2 in the Supporting Information.

To assess the maximum effect of hindered rotations on the rate coefficients, we used the hindered rotor module of the Gaussian 09 program package with the McClurg model,[77−79] as well as the MS-Tor program[80,81] (see section S2.3 in the Supporting Information for more details).

3. RESULTS AND DISCUSSION

For the purposes of this work, we use a practical definition of ELVOC as a very oxidized (at least six O atoms in the structure, i.e., an O/C ratio of >1 in the monomer products, see below) and multifunctional organic compound capable of clustering with the NO_3^- ion.

3.1. Cyclohexene (C_6H_{10}) ELVOC Spectrum. The nitrate chemical ionization mass spectrum of ELVOCs produced in cyclohexene ozonolysis is shown in Figure 1a. The spectrum consists of three highly oxygenated C_6-product species, $C_6H_8O_7$, $C_6H_8O_8$, and $C_6H_8O_9$ (i.e., monomers), below a mass-to-charge ratio (m/z) of 300 Th, separated from each other by the mass of an O atom (15.995 Th) and detected as clusters with NO_3^-. Figure 1b illustrates these same peaks after the addition of D_2O to the bath gas flow (more below on section 3.2.3). Additionally, smaller peaks are seen above 300 Th and are referred to hereafter as "dimers", owing to their

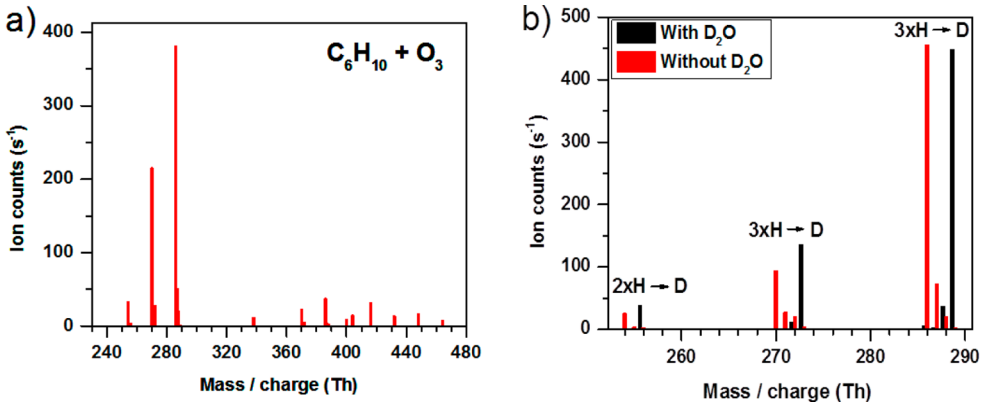

Figure 1. (a) Nitrate CI-APi-TOF mass spectrum showing the ELVOC peaks detected in the cyclohexene ozonolysis system. (b) ELVOC peaks shift after adding D_2O to the gas flow (only monomer range shown).

Table 1. Major ELVOC Species Observed in the Ozonolysis Experiments

Cyclohexene, C_6H_{10}						
$C_6H_{10}O_6$ [a,c] 240.0361 [b]	$C_6H_8O_7$ 254.0154	$C_6H_8O_8$ 270.0103	$C_6H_8O_9$ 286.0052	$C_{12}H_{20}O_7$ 338.1093	$C_{12}H_{20}O_9$ 370.0991	$C_{12}H_{20}O_{10}$ 386.0940
$C_{12}H_{18}O_{11}$ 400.0733	$C_{11}H_{18}O_{12}$ 404.0682	$C_{12}H_{18}O_{12}$ 416.0676	$C_{12}H_{18}O_{13}$ 432.0631	$C_{12}H_{18}O_{14}$ 448.0580	$C_{12}H_{18}O_{15}$ 464.0529	
Cyclohexene-d_{10}, C_6D_{10}						
$C_6D_8H_2O_6$ [c] 248.0863	$C_6D_6H_2O_7$ [d] 260.0530	$C_6D_5H_3O_8$ $C_6D_7HO_8$ $C_6D_8O_8$ 275.0417 277.0542 278.0605	$C_6D_5H_3O_9$ $C_6D_7HO_9$ $C_6D_8O_9$ 291.0366 293.0491 294.0554	$C_{12}D_{18}H_2O_7$ 356.2223	$C_{12}D_{17}HO_8$ 369.1968	$C_{11}D_{16}H_2O_9$ 372.1839
$C_{11}D_{15}H_3O_{10}$ 387.1725 $C_{12}D_{17}H_3O_9$ 387.2058	$C_{12}D_{16}H_2O_{10}$ 400.1772	$C_{12}D_{15}H_3O_{12}$ 431.1623				
***cis*-6-nonenal, $C_9H_{16}O$**						
–	$C_6H_8O_7$ 254.0154	$C_6H_8O_8$ 270.0103	$C_6H_8O_9$ 286.0052			

[a]Identified elemental composition of the peak detected. [b]Mass to charge ratio given in Thomson units; all the peaks detected as clusters with NO_3^-. [c]The only monomer peak that is not explained by the mechanisms of Schemes 1 and 2, most likely produced by OH_2 reaction (see below). [d]Labile D atoms have been exchanged to H atoms prior to detection.

elemental composition. The major peaks observed and their compositions determined are given in Table 1.

It should be emphasized that the determination of final product structures from a mass spectrum is generally ambiguous—multiple isomers could be detected at the same *m*/*z*-signal. Thus, to understand the nature of the highly oxidized products formed, we utilized quantum chemistry, together with a suite of further laboratory experiments, to unravel the chemical identities of the products observed. Evidence gathered from these separate experiments and calculations enabled us to propose product structures for the monomer ELVOCs detected.

3.2. Proposed Cyclohexene ELVOC Formation Scheme. We propose a formation pathway for the monomer ELVOCs detected in C_6H_{10} ozonolysis (Figure 1, Table 1) starting from the $C_6H_9O_4$ peroxy radical (Scheme 2). This scheme is motivated using quantum chemical calculations (section 3.2.1), supporting experiments (sections 3.2.2. to 3.2.4.), and previously suggested autoxidative formation pathways.[12,19]

No experimental rate coefficients were determined during these investigations. Nevertheless, the shortest residence time of 4 s in the flow tube constrains the whole pseudounimolecular autoxidation process to terminate in less than this time.

3.2.1. Computational Results. The most likely H-shift reaction pathways as predicted by our quantum calculations are shown in Scheme 2. The computed reaction rate coefficients for the most important H-shifts of the $C_6H_9O_4$, $C_6H_9O_6$, and $C_6H_9O_8$ peroxy radicals and for the CO loss reactions of the $C_6H_9O_4$, $C_6H_9O_6$ acylic radicals are given in Table 2. For $C_6H_9O_8$, forward rates of two additional minor H-shift channels are given in the Supporting Information. Owing to computational limitations, we were unable to treat the $C_6H_9O_{10}$ radical at the level of theory chosen for this study. The structures,

dx.doi.org/10.1021/ja507146s | J. Am. Chem. Soc. 2014, 136, 15596−15606

Scheme 2. Proposed ELVOC Formation Pathways Starting from the $C_6H_9O_4$ Peroxy Radical in the Cyclohexene Ozonolysis System[a]

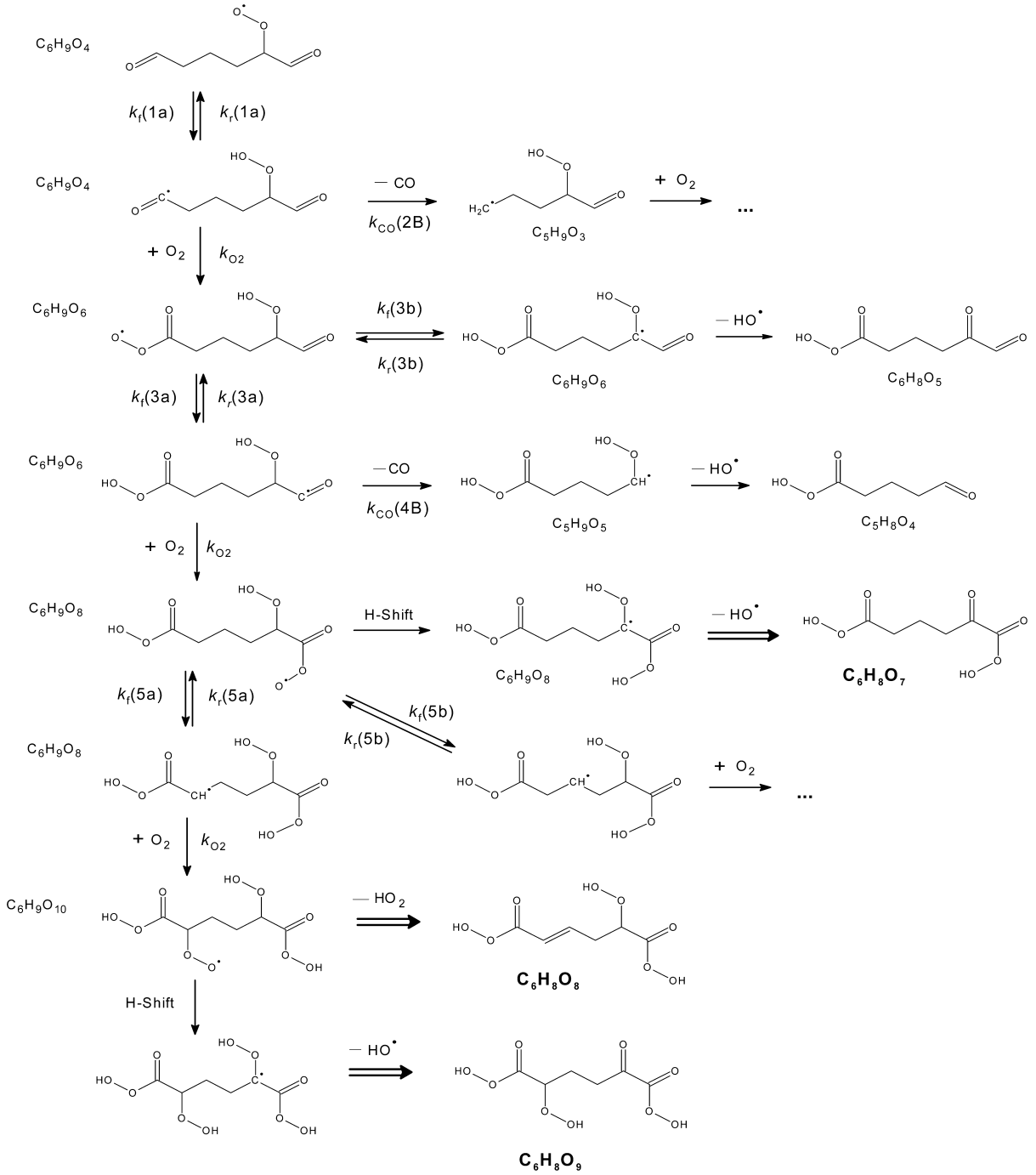

[a]The rate coefficients for the different reversible hydrogen shift reactions (labelled by k_f for forward and k_r for reverse rates), and for the CO loss pathways (k_{CO}), have been obtained by quantum chemical computations and are given in Table 2. The radical chain reaction is propagated until a termination occurs by loss of OH or HO_2 (thick arrows) or by reaction with other peroxy radicals (HO_2 and RO_2, not shown in this scheme). The ELVOCs observed in the nitrate CI-APi-TOF spectra have been marked with bold font.

energetic parameters, and Cartesian coordinates of the lowest-energy conformers are given in section S2.4. of the Supporting Information.

Table 2 shows that in contrast to reactions of unsubstituted peroxy radicals, the hydrogen shift reactions of cyclohexene ozonolysis products are reasonably fast, occurring on a time scale of seconds or less. This is in agreement with recent work on H-shifts in other oxygen-containing molecules.[19] Also, the reactions are thermodynamically either close to thermoneutral or exothermal, leading to low reverse rate coefficients especially for the second and third peroxy radical H-shifts.

The computed results can be used to compare the main unimolecular loss mechanisms. CO loss from the aldehydic carbon-centered radicals competes with irreversible O_2 addition. The rate of the latter is likely close to that of the analogous $CH_3CO + O_2$ reaction, which is around 5×10^{-12}

dx.doi.org/10.1021/ja507146s | J. Am. Chem. Soc. 2014, 136, 15596−15606

Table 2. Calculated MC-TST Rate Coefficients Including Eckart Tunneling Corrections for the Main H-Shift and CO Loss Reactions[a]

label	reaction type	$k_{MC\text{-}TST}$ (s^{-1}) forward, k_f	reverse, k_r
$k_f(1a)$, $k_r(1a)$	1,7 H-shift in $C_6H_9O_4$	7.5	86
k_{O2}	O_2 addition to 1,7 H-shift product of $C_6H_9O_4$	2.5×10^{7}[b]	
$k_{CO}(2B)$	CO loss from 1,7 H-shift product of $C_6H_9O_4$	5.1×10^{2}	
$k_f(3a)$, $k_r(3a)$	1,8 H-shift in $C_6H_9O_6$	0.5	1.3×10^{-6}
$k_f(3b)$ $k_r(3b)$	1,7 H-shift in $C_6H_9O_6$	3.8	1.5×10^{-9}
k_{O2}	O_2 addition to 1,8 H-shift product of $C_6H_9O_6$	2.5×10^{7}[b]	
$k_{CO}(4B)$	CO loss from 1,8 H-shift product of $C_6H_9O_6$	3.3×10^{6}	
$k_f(5a)$, $k_r(5a)$	1,7 H-shift in $C_6H_9O_8$	4.5×10^{-2}	3.8×10^{-4}
$k_f(5b)$, $k_r(5b)$	1,6 H-shift in $C_6H_9O_8$	0.1	1.4

[a]The relative ROHF-RCCSD(T)-F12a/VDZ-F12 energies (energy barriers) between the lowest energy conformers of R, TS, and P and the ωB97XD/aug-cc-pVTZ imaginary frequency have been used for the Eckart tunneling corrections. Hindered rotor corrections are not included; see the SI for discussion of these. [b]Estimated using an O_2 concentration of 0.2 atm and a literature value of 5×10^{-12} cm^3 $molecule^{-1}$ s^{-1} for the O_2 addition reaction.[82]

cm^3 $molecule^{-1}$ s^{-1}.[82] At an O_2 concentration of 0.2 atm, this implies an effective unimolecular rate coefficient of around 2.5×10^7 s^{-1} for the O_2 addition. Thus, CO loss from the $C_6H_9O_4$ carbon-centered radical is completely negligible, and even the very rapid CO loss reaction from $C_6H_9O_6$ is still an order of magnitude slower than the O_2 addition pathway.

On the basis of the computed results, the main unimolecular loss mechanism preventing the formation of C_6-compounds with O/C ratios above 1 is OH loss from the $C_6H_9O_6$ radical following an 1,7 H-shift, leading to a $C_6H_8O_5$ product. (Test calculations at the ωB97XD/aug-cc-pVTZ level indicate that the barrier for OH loss is on the order of 5 kcal/mol, implying that OH loss occurs almost immediately after the H-shift.) The predicted branching ratio for the 1,8 H-shift permitting O_2 addition and further autoxidation is only about 10%. However, the subsequent hydrogen shifts for the $C_6H_9O_8$ peroxy radical favor further oxidation, as the 1,4 H-shift leading to OH loss is predicted to be slower than the H-shifts given in Table 2 (see Table S3 in the SI for a comparison of all four forward rates). Also, the net overall rates for the two H-shifts for $C_6H_9O_8$ shown in Table 2 are likely a factor of 2 higher than the numbers given, because there are two abstractable hydrogens in each CH_2 group (unlike the other H-shifts in the table). Most of the $C_6H_9O_8$ radicals will therefore likely survive to form $C_6H_9O_{10}$ radicals, and thus yield $C_6H_8O_9$ or $C_6H_8O_8$ closed-shell products after loss of OH and HO_2, respectively.

Our calculations thus predict that significant amounts of $C_6H_8O_5$ products should be formed compared to the more highly oxidized ELVOCs. Unfortunately, $C_6H_8O_5$ is probably not detectable by NO_3^- chemical ionization, as it does not bond strongly enough to the NO_3^- ion with its single OOH group.[83]

All in all, the computed rate coefficients are consistent with ELVOC formation proceeding as proposed in Scheme 2. The whole pseudounimolecular sequence of reactions is calculated to complete at time scales of seconds, and is expected to give an ELVOC formation yield on the order of some percent. Figure 2 illustrates the potential energy surface for the proposed ELVOC formation pathway from $C_6H_9O_4$ to $C_6H_9O_8$.

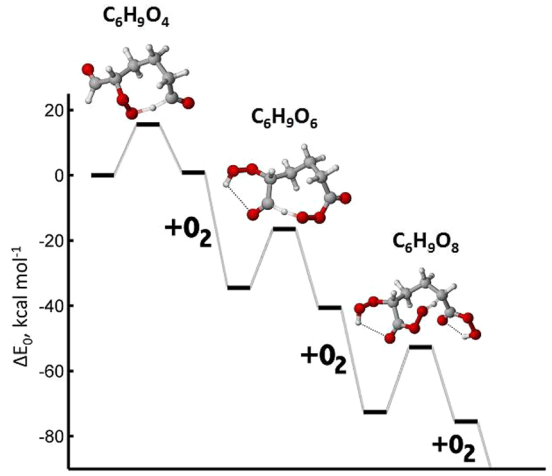

Figure 2. Potential energy surface (zero-point corrected electronic energies at the ROHF-RCCSD(T)-F12a/VDZ-F12//ωB97XD/aug-cc-pVTZ level, in kcal/mol) for the ELVOC-forming pathway. The key transition states are shown schematically. The reference energy level is that of the $C_6H_9O_4$ peroxy radical and free oxygen molecules.

The computed rate coefficients are highly sensitive to the level of quantum chemical theory used. As described in the Experimental Section, relative energies of different conformers are reasonably reliably predicted already by density functional theory with modest basis sets. However, the absolute reaction energetics are not: the CCSD(T)-F12 energy corrections changed barrier heights by up to 5 kcal/mol (implying roughly a factor of 5000 in the rate coefficient). For the hydrogen shift reactions, accounting for tunneling is also important. As shown in Supporting Information, Table S3, tunneling increases the net rate coefficients of H-shifts by between 30 and 700. Accounting for the presence of multiple conformers (by using MC-TST rather than conventional TST) usually decreases, but in a few cases may also increase, the rate coefficient. This effect is always less than a factor of 30 and usually less than a factor of 10. Accounting for hindered rotations tends to decrease both the forward and reverse rate coefficients, depending on the number of internal rotations constrained in the transition states, but this effect is less than a factor of 6 (see section S2.3. in the Supporting Information).

3.2.2. Deuterated Cyclohexene (C_6D_{10}) ELVOC Spectrum. Using fully deuterated cyclohexene (C_6D_{10}), instead of unsubstituted cyclohexene (C_6H_{10}), the postulated hydrogen shift reactions should be seen to slow down due to the primary kinetic isotope effect caused by the heavier D atoms.[84] Transition state theory calculations on the lowest-energy conformers of the three main ELVOC-forming H-shifts indicate that deuteration decreases the H-shift rate coefficients by about a factor of 30 for $C_6H_9O_4$ and $C_6H_9O_6$ peroxy radicals, and by a factor more than 200 for $C_6H_9O_8$. The decrease is due both to a reduction of the tunneling factor and to an increase in the zero-point corrected energy barrier. This should lead to at least four different observable outcomes: (i) the yield of deuterated ELVOC should be smaller than the yield of unsubstituted ELVOC, (ii) the product distribution should show less oxidized species (lower O/C) than with only hydrogen containing cyclohexene ozonolysis, (iii) the dimer distribution should be

dx.doi.org/10.1021/ja507146s | J. Am. Chem. Soc. 2014, 136, 15596−15606

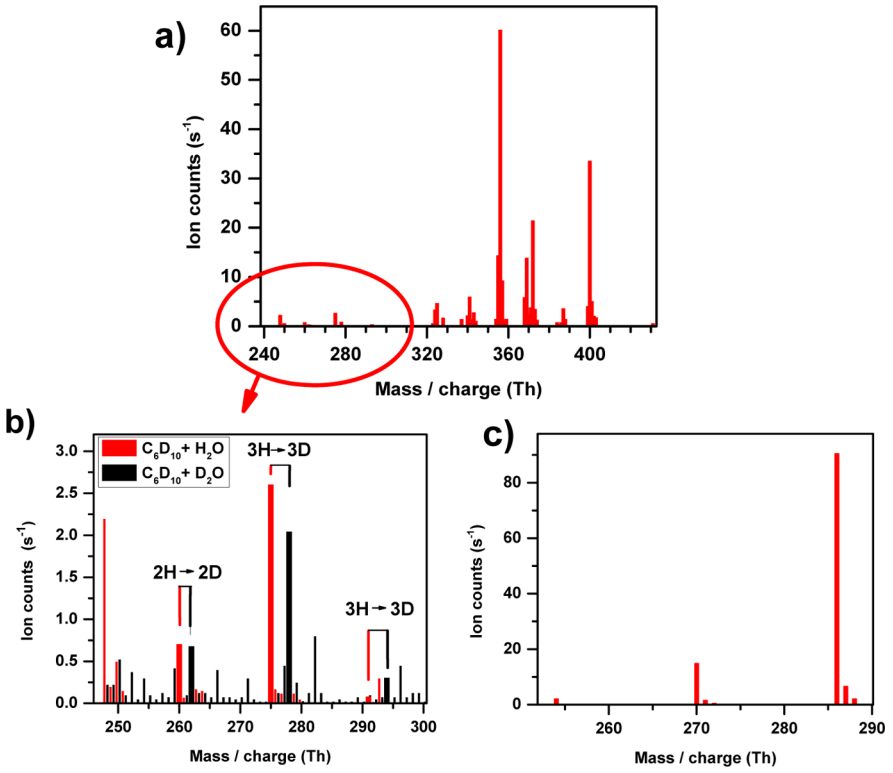

Figure 3. (a–c) ELVOC spectra from the supporting experiments: (a) ELVOC spectrum obtained from the C_6D_{10} + O_3 reaction. Peaks below 300 Th are monomers, and those above 300 Th are dimers; see Table 1 for the elemental compositions of the peaks. (b) Monomer ELVOC spectrum of panel a magnified. The deuterated ELVOC products exchange D → H prior to detection, but adding D_2O to the gas flow exchanges the H → D; the C_6D_{10} + D_2O (+O_3) peaks have been scaled by multiplying them with a factor of 3. (c) ELVOC spectrum obtained from the *cis*-6-nonenal + O_3 experiment, which is nearly identical to the monomer spectrum of cyclohexene (Figure 1).

narrower in the deuterated case, as there are fewer different peroxy radicals in the reaction mixture, and (iv) the dimer to monomer ratio should be higher because of slower unimolecular termination paths. These effects arise as the hydrogen shifts leading to larger oxygen contents are slower with deuterium atoms, and the infusion of O_2 to the carbon structure requires the H/D-shift to create a place for the next O_2 addition.

Indeed these influences are seen in the product distributions (Figure 1, 3a, b, and Table 1). The intensities of the monomer ELVOC peaks observed have dropped roughly by a factor of 100 to 1000 in the fully deuterated system, even though the vapor pressures of C_6H_{10} and C_6D_{10} are similar, and their rate coefficients with O_3 are comparable[29] (note that the deuteration of cyclohexene does not change the O_3 reaction rate significantly, as the C–D bonds do not take part in the primary reaction step). Also the dimer distribution has narrowed and shows less oxidized species (i.e., the heaviest and most oxidized dimer in the C_6H_{10} + O_3 system is found at 464.0529 Th with 15 O atoms attached, whereas the heaviest dimer in the C_6D_{10} + O_3 system has only 12 O atoms and is found at 431.1623 Th; see Table 1). In addition, the dimer to monomer ratio is significantly higher in the deuterated system (compare Figures 1a and 3a), indicating that monomer formation through hydrogen shifts followed by OH or HO_2 elimination is less efficient than dimer formation through peroxy radical recombination in the ozonolysis of C_6D_{10} compared to the C_6H_{10} case (more on dimers in the following sections and in the Supporting Information).

3.2.3. Influence of Water (H_2O or D_2O) on the Cyclohexene ELVOC Spectra. To inspect the ELVOC functionality we added H_2O and D_2O to the carrier gas flow. When H_2O was added, we did not observe changes in the cyclohexene ELVOC signals, (see Figure S2 in the Supporting Information), but when D_2O was used instead, we observed systematic shifts in the m/z of the detected ELVOC, as expected given that labile acidic hydrogens are easily exchanged (e.g., –OH and –OOH, that is, H atoms bonded to electronegative species such as O atom; see Figure 1b and 3b and Figure S3 in the Supporting Information).[29,85−87] That is, a specific number of hydrogens in the ELVOC were substituted to deuterium (H → D), revealing important clues about the structures of the species formed.

Given the high number density of D_2O in the gas mixture, we expected H/D exchange to go to completion, such that the identified ELVOCs will shift one mass unit in the spectrum for every exchangeable hydrogen atom in the ELVOC molecule. In the presence of D_2O, the lightest, major ELVOC product ($C_6H_8O_7$ at 254.0154 Th, see Scheme 2), was observed to shift by two mass units, indicating that 2 H atoms were exchanged to D (Figure 1b). The more oxygenated 270.0103 Th ($C_6H_8O_8$) and 286.0052 Th ($C_6H_8O_9$) products, in contrast, shifted by three mass units (i.e., 3 H were exchanged to D). These observations are consistent with the mechanism in that the third hydroperoxide functionality is not yet formed in the parent compound producing the 254.0154 Th ($C_6H_8O_7$) signal, and support the reaction sequence advancing by H-shifts and creating labile, exchangeable hydrogens (as –OOH) during the process, as described in Scheme 2. However, the effective formation rate of the $C_6H_8O_7$ product through the 1,4-H shift

dx.doi.org/10.1021/ja507146s | J. Am. Chem. Soc. 2014, 136, 15596–15606

of the $C_6H_8O_8$ intermediate was calculated to be only about 0.001 s^{-1} (see Table S3 in the SI), and hence, should not give an appreciable yield in the experimental time-scale. Thus, it seems more likely that $C_6H_8O_7$ product is formed through bimolecular reactions of the intermediate peroxy radials (i.e., by RO_2 + RO_2 reactions discussed below in section 3.3.). Nevertheless, some product formation could be observed even with the calculated formation rate.

3.2.4. cis-6-Nonenal. To further test the general applicability of the proposed mechanism, we performed additional *cis*-6-nonenal ozonolysis experiments, previously reported to produce an ELVOC spectrum.[12] According to general ozonolysis mechanisms of unsaturated organic compounds,[60,61] *cis*-6-nonenal produces the same CI as cyclohexene, but with less internal excitation due to the exocyclic double bond position in 6-nonenal, and with a lesser yield because another three-carbon CI is produced concomitantly (see Scheme S1 in the SI for structures of the nonenal CIs). The *cis*-6-nonenal + O_3 reaction was observed to generate a nearly identical ELVOC monomer distribution to that from cyclohexene + O_3 (compare Figures 1a and 3c), thus lending credit to the suggested formation mechanism (Scheme 2). Also, the addition of D_2O to the gas mixture resulted in similar mass shifts in the spectrum, further crediting the proposition (see Figure S4 in the SI).

3.3. Bimolecular Termination Reactions and Dimer Formation. In addition to unimolecular termination reactions described above, the radical chain can also be terminated by recombination and cross combination reactions of RO_2:[88,89]

$$RO_2 + RO_2 \rightarrow ROOR + O_2 \quad (R1)$$

$$RO_2 + HO_2 \rightarrow ROOH + O_2 \quad (R2)$$

$$RO_2 + RO_2 \rightarrow RO + RO + O_2 \quad (R3)$$

$$RO_2 + RO_2 \rightarrow RCHO + ROH + O_2 \quad (R4)$$

Channels (R1) and (R2) are likely the most relevant for ELVOC formation. However, as the HO_2/RO_2 ratio is small in our flow tube experiments, in contrast to the ambient atmosphere where the opposite usually holds, we do not see products that could be unambiguously assigned to reaction R2. Nevertheless, the product $C_6H_{10}O_6$ (shown in Table 1, but observed with too low intensity to be visible in the scale of Figure 1a), has the expected composition and could be produced through this channel. The alkoxy radicals formed in reaction R3 are potential/common chain branching agents in radical reaction sequences, and hence, are not generally expected to lead to molecular weight growth chemistry, although exceptions (e.g., by isomerization through 1,4 and 1,5 H-shifts) do exist.[17,87,90] The alcohol and carbonyl species created in reaction R4 could in principle be ELVOC compounds, provided that the starting peroxy radicals were oxidized sufficiently before the reaction. The observed $C_6H_8O_7$ product, shortly discussed above, is potentially formed through reaction channel (R4), as its formation rate was found too slow to be produced in appreciable amounts from the autoxidation reaction pathway shown in Scheme 2.

When the O_3 and cyclohexene concentrations are increased enough, dimers appear in the spectra (Figures 1a and 3a, Table 1). These are not conventional dimers held together by van der Waals forces and H-bonds, but instead distinct chemical species formed in reaction R1. The dimers generally have 12 C atoms, either 18 or 20 H atoms and a lower O/C than the monomers (Table 1), which shows their formation being in competition with the unimolecular autoxidative, H-shift + O_2 addition sequence, forming the monomer compounds. In experiments with D_2O, the dimer species generally exchanged an equal or smaller number of hydrogens than the monomer species, and thus indicated different chemical structures (i.e., some of the acidic hydrogens have not formed through H-shifts before a termination has occurred by a bimolecular reaction). The reaction channel (R1) leads to peroxides, which are the likely dimer structures detected in this work. If the recombination or cross-combination reaction occurs between $C_6H_9O_6$ and $C_6H_9O_8$ acylic peroxy radicals, diacyl peroxides are expected to form. More on the specific dimers, their formation, and D-exchange reactions can be found in the Supporting Information.

3.4. ELVOC Yield. The yield of ELVOC from the cyclohexene ozonolysis reaction was determined by varying the reagent cyclohexene and ozone concentrations and measuring the produced ELVOC concentrations with the nitrate CI-APi-TOF. The yield increases linearly with the product of these concentrations (i.e., with [cyclohexene] × [O_3]), as expected for products of a chain process that begins with, and is limited by, the cyclohexene ozonolysis reaction. At the highest reagent concentrations, the yield curve started to bend gradually, and thus only the lowest concentrations were used in the ELVOC yield determination (Figure 4), in order to avoid complication by uncertain second order terms.

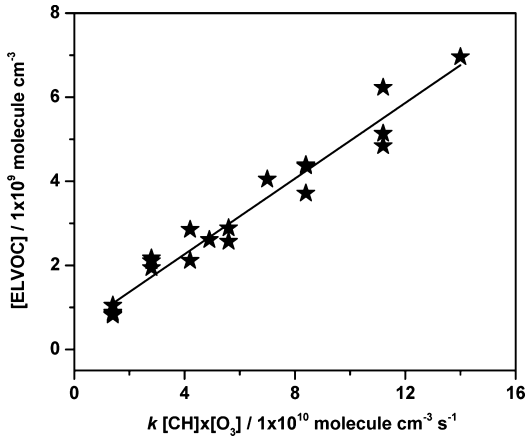

Figure 4. ELVOC yield plot obtained from cyclohexene ozonolysis. Measured ELVOC concentrations follow the product of k × [cyclohexene] × [O_3] ($k(C_6H_{10} + O_3) = 7.4 \times 10^{-17}$ cm^3 $molecule^{-1}$ s^{-1} [33]). Only the identified peaks shown in Table 1 were included.

The detection efficiency of the nitrate CI-APi-TOF to ELVOC was recently estimated to be similar to the detection efficiency of H_2SO_4.[12] Taking into account the calibration factor for H_2SO_4 determined in this work (see the Supporting Information), together with an estimated diffusion limited wall loss for the sticky ELVOC molecules, one arrives at an ELVOC yield of (4.5 ± 0.2)% from the C_6H_{10} + O_3 reaction (Figure 4), with the uncertainty given as one standard error of the fit. The overall uncertainty of this value was estimated as ±80%, and was obtained by the propagation of error method. The agreement with the only previous determination of Ehn et al.,[12] (4 ± 2)%, obtained under very different experimental conditions in the Jülich Plant Atmosphere Chamber (JPAC), is excellent. For the C_6D_{10} + O_3 reaction, appreciable ELVOC signals were obtained only with the highest reagent concentrations used, and hence, the ELVOC yield could not

dx.doi.org/10.1021/ja507146s | J. Am. Chem. Soc. 2014, 136, 15596−15606

be determined similarly as in the $C_6H_{10} + O_3$ reaction. It can, however, be roughly estimated as about 2 orders of magnitude lower, leading to a value of about 0.04%. More details of the yield experiments and calculation are given in the Supporting Information.

It must be emphasized that the yield determined in this work corresponds only to a few percent of the total $C_6H_{10} + O_3$ product yield and does not contradict the formation of already well-established major products of the reaction.[29−57] Nevertheless, even such a small yield can have significant consequences on the formation of SOA, as was shown by Ehn et al.[12]

4. CONCLUSIONS

The formation of highly oxidized, extremely low volatility products from the ozonolysis of cyclohexene was investigated by experimental and computational methods. A large amount of previously unidentified product species, with O/C ratios as high as 1.5, were detected in the nitrate chemical ionization mass spectra. Results of quantum chemical calculations, supplemented by additional specific laboratory experiments, enabled us to assign chemical structures for the measured elemental compositions. The ELVOC yield from the cyclohexene ozonolysis system was estimated to be (4.5 ± 3.8)%.

Gas-phase oxidation chemistry advancing by peroxy radical H-shift + O_2 addition has been reported previously. However, owing to the lack of experimental tools to detect the highly oxidized and extremely low volatility products of these reactions, the sequence of reactions has not been recognized to advance as far as what is found here (and implicated by very recent research). In addition, the time scale in which these reactions form closed-shell ELVOC products is much shorter than previously thought, the whole process starting and terminating in seconds or less.

The results of the current study have potentially important consequences for the understanding of atmospheric SOA formation processes. In the current work, cyclohexene was specifically chosen as a surrogate for many biogenic VOCs with endocyclic double bonds, to gain insight into ELVOC formation from ozonolysis. The simpler structure of cyclohexene allowed high-level quantum chemical calculations of the detailed step-by-step progression of rapid oxygenation of the precursor compound. This progression, with rate coefficients for favorable H-abstraction sites and typical radical termination reactions, provides a starting point for interpreting the more complex ELVOC spectra produced from important biogenic emissions, such as mono- and sesquiterpenes, crucial precursors for atmospheric SOA.

■ ASSOCIATED CONTENT

Supporting Information

Sections S1.1−S1.9, additional information on performed laboratory experiments; Figure S1, experimental setup, Figure S2 H_2O influence on ELVOC signals, Figure S3 D_2O influence on ELVOC signals. Scheme S1, Criegee intermediates from *cis*-6-nonenal ozonolysis. Table S1, description of the experiments performed; sections S2.1.−S2.4., additional details on quantum chemical calculations; Figures S5−S7, Lowest-energy structures for the $C_6H_9O_4$, $C_6H_9O_6$, and $C_6H_9O_8$; Table S2, partition functions of the reactants, transition states and products for each reaction; Table S3, calculated rate coefficients for the different H-shift and CO loss reactions; Table S4, thermodynamic properties of the structures shown in Figures S5−S7; Table S5, Cartesian coordinates of the structures shown in Figures S5−S7; Tables S6−S22 conformers of the species used in the final quantum chemical calculations. This material is available free of charge via the Internet at http://pubs.acs.org.

■ AUTHOR INFORMATION

Corresponding Author

matti.p.rissanen@helsinki.fi

Notes

The authors declare no competing financial interest.

■ ACKNOWLEDGMENTS

T.K. and M. Sipilä thank the Academy of Finland for funding (Academy Research Fellow Grant No. 266388 and Post Doctoral Researcher Grant No. 251427, respectively). H.G.K. acknowledges the support from The Danish Council for Independent Research—Natural Sciences and the Danish Center for Scientific Computing. J.A.T. acknowledges support from the U.S. Department of Energy through Grants DE-SC0011791 and DE-SC0006867. We thank Markku Kulmala for providing the instrumentation and laboratory facilities used in this work. We thank the CSC IT Center for Science in Espoo, Finland for computing resources.

■ REFERENCES

(1) Kulmala, M.; Kontkanen, J.; Junninen, H.; Lehtipalo, K.; Manninen, H. E.; Nieminen, T.; Petaja, T.; Sipila, M.; Schobesberger, S.; Rantala, P.; Franchin, A.; Jokinen, T.; Järvinen, E.; Äijälä, M.; Kangasluoma, J.; Hakala, J.; Aalto, P.; Paasonen, P.; Mikkilä, J.; Vanhanen, J.; Aalto, J.; Hakola, H.; Makkonen, U.; Ruuskanen, T.; Mauldin, R. L., III.; Duplissy, J.; Vehkamaki, H.; Back, J.; Kortelainen, A.; Riipinen, I.; Kurten, T.; Johnston, M. V.; Smith, J. N.; Mikael, E.; Mentel, T. F.; Lehtinen, K. E. J.; Laaksonen, A.; Kerminen, V.-M.; Worsnop, D. R. *Science* **2013**, *339*, 943−946.

(2) Zhang, Q.; Jimenez, J. L.; Canagaratna, M. R.; Allan, J. D.; Coe, H.; Ulbrich, I.; Alfarra, M. R.; Takami, A.; Middlebrook, A. M.; Sun, Y. L.; Dzepina, K.; Dunlea, E.; Docherty, K.; DeCarlo, P. F.; Salcedo, D.; Onasch, T.; Jayne, J. T.; Miyoshi, T.; Shimono, A.; Hatakeyama, S.; Takegawa, N.; Kondo, Y.; Schneider, J.; Drewnick, F.; Borrmann, S.; Weimer, S.; Demerjian, K.; Williams, P.; Bower, K.; Bahreini, R.; Cottrell, L.; Griffin, R. J.; Rautiainen, J.; Sun, J. Y.; Zhang, Y. M.; Worsnop, D. R. *J. Geophys Res.* **2007**, *34*, L13801−6.

(3) Jimenez, J. L.; Canagaratna, M. R.; Donahue, N. M.; Prevot, A. S.; Zhang, Q.; Kroll, J. H.; DeCarlo, P. F.; Allan, J. D.; Coe, H.; Ng, N. L.; Aiken, A. C.; Docherty, K. S.; Ulbrich, I. M.; Grieshop, A. P.; Robinson, A. L.; Duplissy, J.; Smith, J. D.; Wilson, K. R.; Lanz, V. A.; Hueglin, C.; Sun, Y. L.; Tian, J.; Laaksonen, A.; Raatikainen, T.; Rautiainen, J.; Vaattovaara, P.; Ehn, M.; Kulmala, M.; Tomlinson, J. M.; Collins, D. R.; Cubison, M. J.; Dunlea, E. J.; Huffman, J. A.; Onasch, T. B.; Alfarra, M. R.; Williams, P. I.; Bower, K.; Kondo, Y.; Schneider, J.; Drewnick, F.; Borrmann, S.; Weimer, S.; Demerjian, K.; Salcedo, D.; Cottrell, L.; Griffin, R.; Takami, A.; Miyoshi, T.; Hatakeyama, S.; Shimono, A.; Sun, J. Y.; Zhang, Y. M.; Dzepina, K.; Kimmel, J. R.; Sueper, D.; Jayne, J. T.; Herndon, S. C.; Trimborn, A. M.; Williams, L. R.; Wood, E. C.; Middlebrook, A. M.; Kolb, C. E.; Baltensperger, U.; Worsnop, D. R. *Science* **2009**, *326*, 1525−1529.

(4) *IPCC 5th Assessement Report*; Intergovernmental Panel on Climate Change: Paris, France, 2013; http://www.ipcc.ch/report/ar5/.

(5) Ng, N. L.; Canagaratna, M. R.; Zhang, Q.; Jimenez, J. L.; Tian, J.; Ulbrich, I. M.; Kroll, J. H.; Docherty, K. S.; Chhabra, P. S.; Bahreini, R.; Murphy, S. M.; Seinfeld, J. H.; Hildebrandt, L.; Donahue, N. M.; DeCarlo, P. F.; Lanz, V. A.; Prévôt, A. S. H.; Dinar, E.; Rudich, Y.; Worsnop, D. R. *Atmos. Chem. Phys.* **2010**, *10*, 4625−4641.

(6) Aiken, A. C.; DeCarlo, P. F.; Kroll, J. H.; Worsnop, D. R.; Huffman, J. A.; Docherty, K. S.; Ulbrich, I. M.; Mohr, C.; Kimmel, J.

R.; Sueper, D.; Sun, Y.; Zhang, Q.; Trimborn, A.; Northway, M.; Ziemann, P. J.; Canagaratna, M. R.; Onasch, T. B.; Alfarra, M. R.; Prévôt, A. S. H.; Dommen, J.; Duplissy, J.; Metzger, A.; Baltensperger, U.; Jimenez, J. L. *Environ. Sci. Technol.* **2008**, *42*, 4478−4485.
(7) Kroll, J. H.; Seinfeld, J. H. *Atmos. Environ.* **2008**, *42*, 3593−3624.
(8) Chacon-Madrid, H. J.; Donahue, N. M. *Atmos. Chem. Phys.* **2011**, *11*, 10553−10563.
(9) Donahue, N. M.; Kroll, J. H.; Pandis, S. N.; Robinson, A. L. *Atmos. Chem. Phys.* **2012**, *12*, 615−634.
(10) Donahue, N. M.; Trump, E. R.; Pierce, J. R.; Kulmala, M. *Geophys. Res. Lett.* **2011**, *38*, L16801.
(11) Donahue, N. M.; Ortega, I. K.; Chuang, W.; Riipinen, I.; Riccobono, F.; Schobesberger, S.; Dommen, J.; Baltensperger, U.; Kulmala, M.; Worsnop, D. R.; Vehkamaki, H. *Faraday Discuss.* **2013**, *165*, 91−104.
(12) Ehn, M.; Thornton, J. A.; Kleist, E.; Sipilä, M.; Junninen, H.; Pullinen, I.; Springer, M.; Rubach, F.; Tillmann, R.; Lee, B.; Lopez-Hilfiker, F.; Andres, S.; Acir, I.-H.; Rissanen, M.; Jokinen, T.; Schobesberger, S.; Kangasluoma, J.; Kontkanen, J.; Nieminen, T.; Kurtén, T.; Nielsen, L. B.; Jørgensen, S.; Kjaergaard, H. G.; Canagaratna, M.; Dal Maso, M.; Berndt, T.; Petäjä, T.; Wahner, A.; Kerminen, V.-M.; Kulmala, M.; Worsnop, D. R.; Wildt, J.; Mentel, T. F. *Nature* **2014**, *506*, 476−479.
(13) Kulmala, M.; Toivonen, A.; Mäkelä, J. M.; Laaksonen, A. *Tellus B* **1998**, *50*, 449−462.
(14) Glowacki, D. R.; Pilling, M. J. *ChemPhysChem* **2010**, *11*, 3836−3843.
(15) Taatjes, C. A. *J. Phys. Chem. A* **2006**, *110*, 4299−4312.
(16) Pilling, M. J. *Chem. Soc. Rev.* **2008**, *37*, 676−685.
(17) Vereecken, L.; Francisco, J. S. *Chem. Soc. Rev.* **2012**, *41*, 6259−6293.
(18) Eddingsaas, N. C.; Loza, C. L.; Yee, L. D.; Seinfeld, J. H.; Wennberg, P. O. *Atmos. Chem. Phys.* **2012**, *12*, 6489−6504.
(19) Crounse, J. D.; Nielsen, L. B.; Jørgensen, S.; Kjaergaard, H. G.; Wennberg, P. O. *J. Phys. Chem. Lett.* **2013**, *4*, 3513−3520.
(20) Crounse, J. D.; Knap, H. C.; Ørnsø, K. B.; Jørgensen, S.; Paulot, F.; Kjaergaard, H. G.; Wennberg, P. O. *J. Phys. Chem. A* **2012**, *116*, 5756−5762.
(21) Crounse, J. D.; Paulot, F.; Kjaergaard, H. G.; Wennberg, P. O. *Phys. Chem. Chem. Phys.* **2011**, *13*, 13607−13613.
(22) Mattill, H. A. *Oil Soap* **1941**, *18*, 73−76.
(23) Amorati, R.; Foti, M. C.; Valgimigli, L. *J. Agric. Food Chem.* **2013**, *61*, 10835−10847.
(24) Karlberg, A.-T.; Börje, A.; Johansen, J. D.; Lidén, C.; Rastogi, S.; Roberts, D.; Uter, W.; White, I. R. *Contact Dermatitis* **2013**, *69*, 323−334.
(25) Vereecken, L.; Muller, J. F.; Peeters, J. *Phys. Chem. Chem. Phys.* **2007**, *9*, 5241−5248.
(26) Zhao, J.; Ortega, J.; Chen, M.; McMurry, P. H.; Smith, J. N. *Atmos. Chem. Phys.* **2013**, *13*, 7631−7644.
(27) Ehn, M.; Kleist, E.; Junninen, H.; Petäjä, T.; Lönn, G.; Schobesberger, S.; Dal Maso, M.; Trimborn, A.; Kulmala, M.; Worsnop, D. R.; Wahner, A.; Wildt, J.; Mentel, Th. F. *Atmos. Chem. Phys.* **2012**, *12*, 5113−5127.
(28) Ehn, M.; Junninen, H.; Petäjä, T.; Kurtén, T.; Kerminen, V.-M.; Schobesberger, S.; Manninen, H. E.; Ortega, I. K.; Vehkamäki, H.; Kulmala, M.; Worsnop, D. R. *Atmos. Chem. Phys.* **2010**, *10*, 8513−8530.
(29) Aschmann, S. M.; Tuazon, E. C.; Arey, J.; Atkinson, R. *J. Phys. Chem. A* **2003**, *107*, 2247−2255.
(30) Chuong, B.; Zhang, J.; Donahue, N. M. *J. Am. Chem. Soc.* **2004**, *126*, 12363−12373.
(31) Keywood, M. D.; Kroll, J. H.; Varutbangkul, V.; Bahreini, R.; Flaglan, R. C.; Seinfeld, J. H. *Environ. Sci. Technol.* **2004**, *38*, 3343−3350.
(32) Ziemann, P. *J. Phys. Chem. A* **2002**, *106*, 4390−4402.
(33) Carlsson, P. T. M.; Dege, J. E.; Keunecke, C.; Krüger, B. C.; Wolf, J. L.; Zeuch, T. *Phys. Chem. Chem. Phys.* **2012**, *14*, 11695−11705.
(34) Hamilton, J. F.; Lewis, A. C.; Reynolds, J. C.; Carpenter, L. J.; Lubben, A. *Atmos. Chem. Phys.* **2006**, *6*, 4973−4984.
(35) Drozd, G. T.; Donahue, N. M. *J. Phys. Chem. A* **2011**, *115*, 4381−4387.
(36) Donahue, N. M.; Drozd, G. T.; Epstein, S. A.; Presto, A. A.; Kroll, J. H. *Phys. Chem. Chem. Phys.* **2011**, *13*, 10848−10857.
(37) Atkinson, R.; Aschmann, S. M. *Environ. Sci. Technol.* **1993**, *27*, 1357−1363.
(38) Fenske, J. D.; Kuwata, K. T.; Houk, K. N.; Paulson, S. E. *J. Phys. Chem. A* **2000**, *104*, 7246−7254.
(39) Epstein, S. A.; Donahue, N. M. *J. Phys. Chem. A* **2010**, *114*, 7509−7515.
(40) Stokes, G. Y.; Chen, E. H.; Walter, S. R.; Geiger, F. M. *J. Phys. Chem. A* **2009**, *113*, 8985−8993.
(41) Warren, B.; Austin, R. L.; Cocker, D. R., III. *Atmos. Environ.* **2009**, *43*, 3548−3555.
(42) Warren, B.; Malloy, Q. G. J.; Yee, L. D.; Cocker, D. R., III. *Atmos. Environ.* **2009**, *43*, 1789−1795.
(43) Stokes, G. Y.; Buchbinder, A. M.; Gibbs-Davis, J. M.; Scheidt, K. A.; Geiger, F. M. *J. Phys. Chem. A* **2008**, *112*, 11688−11698.
(44) Nørgaard, A. W.; Nøjgaard, J. K.; Clausen, P. A.; Wolkoff, P. *Chemosphere* **2008**, *70*, 2032−2038.
(45) Shepherd, T. G.; Jonsson, A. I. *Atmos. Chem. Phys.* **2008**, *8*, 1435−1444.
(46) Nøjgaard, J. K.; Nørgaard, A. W.; Wolkoff, P. *Atmos. Environ.* **2007**, *41*, 8345−8354.
(47) Narukawa, M.; Matsumi, Y.; Matsumoto, J.; Takahashi, K.; Yabushita, A.; Sato, K.; Imamura, T. *Anal. Sci.* **2007**, *23*, 507−512.
(48) Gao, S.; Ng, N. L.; Keywood, M.; Varutbangkul, V.; Bahreini, R.; Nenes, A.; He, J.; Yoo, K. Y.; Beauchamp, J. L.; Hodyss, R. P.; Flaglan, R. C.; Seinfeld, J. H. *Environ. Sci. Technol.* **2004**, *38*, 6582−6589.
(49) Gao, S.; Keywood, M.; Ng, N. L.; Surratt, J.; Varutbangkul, V.; Bahreini, R.; Flagan, R. C.; Seinfeld, J. H. *J. Phys. Chem. A* **2004**, *108*, 10147−10164.
(50) Presto, A. A.; Donahue, N. M. *J. Phys. Chem. A* **2004**, *108*, 9096−9104.
(51) Ziemann, P. J. *J. Phys. Chem. A* **2003**, *107*, 2048−2060.
(52) Bailey, P. S. *Ind. Eng. Chem.* **1958**, *50*, 993−996.
(53) Bailey, P. S. *J. Org. Chem.* **1957**, *22*, 1548−1551.
(54) Eastman, R. H.; Silverstein, R. M. *J. Am. Chem. Soc.* **1953**, *75*, 1493−1494.
(55) Müller, L.; Reinnig, M.-C.; Warnke, J.; Hoffmann, Th. *Atmos. Chem. Phys.* **2008**, *8*, 1423−1433.
(56) Kalberer, M.; Yu, J.; Cocker, D. R.; Flagan, R. C.; Seinfeld, J. H. *Environ. Sci. Technol.* **2000**, *34*, 4894−4901.
(57) Hatakeyama, S.; Tanonaka, T.; Weng, J.; Bandow, H.; Takagi, H.; Akimoto, H. *Environ. Sci. Technol.* **1985**, *19*, 935−942.
(58) Johnson, D.; Marston, G. *Chem. Soc. Rev.* **2008**, *37*, 699−716.
(59) Taatjes, C. A.; Shallcross, D. E.; Percival, C. J. *Phys. Chem. Chem. Phys.* **2014**, *16*, 1704−1718.
(60) Criegee, R. *Angew. Chem., Int. Ed. Engl.* **1975**, *14*, 745−752.
(61) Marston, G. *Science* **2012**, *335*, 178−179.
(62) Jokinen, T.; Sipilä, M.; Junninen, H.; Ehn, M.; Lönn, G.; Hakala, J.; Petäjä, T.; Mauldin, R. L., III; Kulmala, M.; Worsnop, D. R. *Atmos. Chem. Phys.* **2012**, *12*, 4117−4125.
(63) Junninen, H.; Ehn, M.; Petäjä, T.; Luosujärvi, L.; Kotiaho, T.; Kostiainen, R.; Rohner, U.; Gonin, M.; Fuhrer, K.; Kulmala, M.; Worsnop, D. R. *Atmos. Meas. Technol.* **2010**, *3*, 1039−1053.
(64) Graus, M.; Müller, M.; Hansel, A. *J. Am. Soc. Mass Spectrom.* **2010**, *21*, 1037−1044.
(65) Jordan, A.; Haidacher, S.; Hanel, G.; Hartungen, E.; Märk, L.; Seehauser, S.; Schottkowsky, R.; Sulzer, P.; Märk, T. D. *Int. J. Mass Spectrom.* **2009**, *286*, 122−128.
(66) Taipale, R.; Ruuskanen, T. M.; Rinne, J.; Kajos, M. K.; Hakola, H.; Pohja, T.; Kulmala, M. *Tech. Note: Atmos. Chem. Phys.* **2008**, *8*, 9435−9475.
(67) Vereecken, L.; Nguyen, T. L.; Hermans, I.; Peeters, J. *Chem. Phys. Lett.* **2004**, *393*, 432−436.

(68) (a) *Spartan'08*; Wavefunction Inc.: Irivine CA, 2008. (b) *Spartan'10*; Wavefunction Inc.: Irivine CA, 2011. (c) *Spartan'14*; Wavefunction Inc.: Irivine CA, 2014.
(69) Garden, A. L.; Paulot, F.; Crounse, J. D.; Maxwell-Cameron, I. J.; Wennberg, P. O.; Kjaergaard, H. G. *Chem. Phys. Lett.* **2009**, *474*, 45−50.
(70) Chai, J.-D.; Head-Gordon, M. *Phys. Chem. Chem. Phys.* **2008**, *10*, 6615−6620.
(71) Frisch, M. J.; Trucks, G. W.; Schlegel, H. B.; Scuseria, G. E.; Robb, M. A.; Cheeseman, J. R.; Scalmani, G.; Barone, V.; Mennucci, B.; Petersson, G. A.; Nakatsuji, H.; Caricato, M.; Li, X.; Hratchian, H. P.; Izmaylov, A. F.; Bloino, J.; Zheng, G.; Sonnenberg, J. L.; Hada, M.; Ehara, M.; Toyota, K.; Fukuda, R.; Hasegawa, J.; Ishida, M.; Nakajima, T.; Honda, Y.; Kitao, O.; Nakai, H.; Vreven, T.; Montgomery, J. A., Jr.; Peralta, J. E.; Ogliaro, F.; Bearpark, M.; Heyd, J. J.; Brothers, E.; Kudin, K. N.; Staroverov, V. N.; Kobayashi, R.; Normand, J.; Raghavachari, K.; Rendell, A.; Burant, J. C.; Iyengar, S. S.; Tomasi, J.; Cossi, M.; Rega, N.; Millam, N. J.; Klene, M.; Knox, J. E.; Cross, J. B.; Bakken, V.; Adamo, C.; Jaramillo, J.; Gomperts, R.; Stratmann, R. E.; Yazyev, O.; Austin, A. J.; Cammi, R.; Pomelli, C.; Ochterski, J. W.; Martin, R. L.; Morokuma, K.; Zakrzewski, V. G.; Voth, G. A.; Salvador, P.; Dannenberg, J. J.; Dapprich, S.; Daniels, A. D.; Farkas, Ö.; Foresman, J. B.; Ortiz, J. V.; Cioslowski, J.; Fox, D. J. *Gaussian 09*, revision D.01; Gaussian, Inc.: Wallingford CT, 2009.
(72) Adler, T. B.; Knizia, G.; Werner, H.-J. *J. Chem. Phys.* **2007**, *127*, 221106(1−4).
(73) Peterson, K. A.; Adler, T. B.; Werner, H.-J. *J. Chem. Phys.* **2008**, *128*, 084102(1−12).
(74) Werner, H.-J.; Knowles, P. J.; Manby, F. R.; Schütz, M.; Celani, P.; Knizia, G.; Korona, T.; Lindh, R.; Mitrushenkov, A.; Rauhut, G.; Shamasundar, K. R.; Adler, T. B.; Amos, R. D.; Bernhardsson, A.; Berning, A.; Cooper, D. L.; Deegan, M. J. O.; Dobbyn, A. J.; Eckert, F.; Goll, E.; Hampel, C.; Hesselmann, A.; Hetzer, G.; Hrenar, T.; Jansen, G.; Köppl, C.; Liu, Y.; Lloyd, A. W.; Mata, R. A.; May, A. J.; McNicholas, S. J.; Meyer, W.; Mura, M. E.; Nicklaß, A.; O'Neill, D. P.; Palmieri, P.; Peng, D.; Pflüger, K.; Pitzer, R.; Reiher, M.; Shiozaki, T.; Stoll, H.; Stone, A. J.; Tarroni, R.; Thorsteinsson, T.; Wang, M., *MOLPRO, a Package of ab Initio Programs*, version 2010.1; University College Cardiff Consultants Limited: Cardiff, Wales, 2010; http://www.molpro.net.
(75) Vereecken, L.; Peeters, J. *J. Chem. Phys.* **2003**, *119*, 5159−5170.
(76) Eckart, C. *Phys. Rev.* **1930**, *35*, 1303−1309.
(77) Ayala, P. Y.; Schlegel, H. B. *J. Chem. Phys.* **1998**, *108*, 2314−2325.
(78) McClurg, R. B.; Flagan, R. C.; Goddard, W. A., III *J. Chem. Phys.* **1997**, *106*, 6675−6680.
(79) McClurg, R. B. *J. Chem. Phys.* **1999**, *111*, 7163.
(80) Zheng, J.; Mielke, S. L.; Clarkson, K. L.; Truhlar, D. G. *Comput. Phys. Commun.* **2012**, *183*, 1803−1812.
(81) Zheng, J.; Meana-Pañeda, R.; Trular, D. G. *Comput. Phys. Commun.* **2013**, *184*, 2032−2033.
(82) Atkinson, R.; Baulch, D. L.; Cox, R. A.; Hampson, R. F., Jr.; Kerr, J. A.; Rossi, M. J.; Troe, J. *J. Phys. Chem. Ref. Data* **1997**, *26*, 521−1011.
(83) Hyttinen, N.; Rissanen, M. P.; Muuronen, M.; Kupiainen-Määttä, O.; Ehn, M.; Kurtén, T. in preparation.
(84) Benson, S. W. *Thermochemical Kinetics*, 2nd ed.; John Wiley & Sons: New York, U.S.A., 1976.
(85) Wine, P. H.; Astalos, R. J.; Mauldin, R. L., III *J. Phys. Chem.* **1985**, *89*, 2620−2624.
(86) Vaghjiani, G. L.; Ravishankara, A. R. *J. Phys. Chem.* **1989**, *93*, 1948−1959.
(87) Atkinson, R.; Kwok, E. S. C.; Arey, J.; Aschmann, S. M. *Faraday Discuss.* **1995**, *100*, 23−37.
(88) Orlando, J. J.; Tyndall, G. S. *Chem. Soc. Rev.* **2012**, *41*, 6294−6317.
(89) Hasson, A. S.; Tyndall, G. S.; Orlando, J. J. *J. Phys. Chem. A* **2004**, *108*, 5979−5989.
(90) Orlando, J. J.; Tyndall, G. S.; Wallington, T. J. *Chem. Rev.* **2003**, *103*, 4657−4689.